Simplified Channel Model for Simulation of Free-Space Optical Communications

Bernhard Epple

***Abstract*—Free-space optical (or optical wireless) communications represent an attractive technology for the realization of high-bandwidth wireless communications. However, for propagation through the atmosphere the characteristics of the optical signal are different from those of the signals from, e.g., fiber channels or radio-frequency wireless channels, and therefore the error characteristics on these links are also different. For evaluating fading mitigation techniques for optical wireless communications a channel model is needed that can be easily used by protocol designers. Existing channel models for optical wireless communications are based on atmospheric propagation theory and therefore require a deep physical understanding of the optical propagation through the atmosphere. The goal of this publication is to develop a simplified approach for modeling the received power dynamics of the atmospheric free-space optical channel. The proposed model consists of a random number generator and a low-pass filter and is therefore easy to implement and use. This approach is only valid for systems utilizing intensity modulation with direct detection, but this limitation is acceptable since most commercially available systems use this modulation format. The channel model is developed based on the statistics of received power measurements from a maritime-mobile link, a land-mobile link, and a satellite downlink.**

***Index Terms*—Free-space optical communications; Channel model; Measurements; Protocol design; Fading; Mitigation**.

I. INTRODUCTION

Optical wireless communications already have wide acceptance as a complementary technology to near-ground radio-frequency wireless short-range connections, but optical wireless communications can also be used over longer link distances as has already been demonstrated in, for example, the following: in the project CAPANINA a 60 km downlink from a stratospheric platform has been demonstrated [1], in the project KIODO a downlink from a low-Earth-orbiting satellite has been shown [2], and in [3] a 150 km long link between two Hawaiian islands is reported. On free-space optical (FSO) links the received signal is influenced by several system-inherent effects (fading, induced by the pointing and tracking system) as well as several physical effects (scintillation, caused by atmospheric turbulence). The atmospheric effects cause temporal and spatial fluctuations of the received signal [4,5], which, e.g., are responsible for the twinkling of the stars. For shorter ranges it is possible to compensate the scintillation by increasing the transmission power. If the link distance is increased to distances longer than several kilometers, laser safety regulations and technical limitations no longer allow for increasing the transmission power to the required level. In this case fading mitigation techniques (FMT) are needed for error protection of the data stream [6]. In this publication FMT are limited to protocols and coding techniques, despite the fact that it is also possible to mitigate fading on the physical layer by using wavelength diversity [7], multiple transmit beams [8], multiple receivers, and others [9]. The mentioned techniques can only reduce the impact of scintillation and cannot guarantee an error-free channel; therefore additional FMT are required on a higher layer.

For the development of efficient FMT for FSO communications a channel model is needed for conducting simulations. The atmospheric effects on the laser beam are well described by the extended Rytov theory [5]. This theory can be used for the calculation of the probability density function (PDF) of the received power P_{Rx} on the basis of several characterizing atmospheric turbulence parameters. The required parameters are dependent on physical measures such as

Manuscript received February 12, 2010; accepted March 28, 2010; published April 30, 2010 (Doc. ID 123898).

The author is with the Satellite Communications Group of the Institute of Communications and Navigation, German Aerospace Center (DLR), Oberpfaffenhofen, 82234 Wessling, Germany, and the Ludwig Maximilians University Munich, Institute of Computer Science, Oettingenstrasse 67, 80538 München, Germany (e-mail: bernhard.epple@dlr.de).

Digital Object Identifier 10.1364/JOCN.2.000293

temperature, relative humidity, time of day, wind speed, path height above the ground, and others. To determine this high number of different parameters is not a trivial task for most communication scenarios. Additionally, the physical parameters can vary over time and their values do not have to be constant along the link path, which results in a large number of different parameter sets for every scenario under investigation. The problem of determining the exact parameter sets and the variance of possible values make it difficult to use the extended Rytov theory for simulations of optical wireless link performance. For an efficient way to simulate FSO communications it is necessary to reduce the number of the variable parameters contained in the model. This can be achieved by using a statistical description of P_{Rx} rather than by modeling the different physical effects. This statistical description can be derived from measurements of the received power distribution and the power spectral density (PSD). Most commercially available FSO systems are based on intensity modulation with direct detection (IM/DD) using on–off keying (OOK) or pulse position modulation; therefore the focus of this work is on modeling the channel for such systems and only amplitude statistics of the received signal are investigated.

The remaining part of this publication is structured as follows. In Section II it is evaluated which PDF can be used to model the distribution of P_{Rx}. For this evaluation, PDFs proposed in the literature are compared against measurements from three successful FSO demonstrations. The available data sets are from a land-mobile link, a maritime-mobile link, and a satellite downlink. The scenarios are described in more detail in Subsection II.D. Then in Section III the measured data is further analyzed to derive a description of the PSD of P_{Rx}. In Section IV the gathered results are put together to form a simplified model for FSO communications. Finally the findings of this work are discussed in Section V.

II. Probability Density Functions for the Received Optical Power

Over the years several PDFs have been proposed to characterize the intensity of the received optical signal. For the weak scintillation regime the log-normal (LN) distribution is widely accepted as the characterizing distribution [4,10]. For the PDF under moderate to strong scintillation the LN distribution was also widely accepted until additional work [11,12] showed that the LN assumption is not valid under certain conditions, especially if turbulence increases and moderate to strong scintillation is experienced. For this case the K, gamma (G), and gamma-gamma (GG) distributions are reported as suitable PDFs [4,10,13], where the GG distribution is a generalization of the K distribution and should be valid under weak scintillation as well as under moderate to strong scintillation.

As long as the receiving aperture is small enough and therefore no aperture averaging is taking place, the distribution of the normalized received intensity is equivalent to the normalized received power. This does not hold if aperture averaging takes place. For the case of aperture averaging the LN distribution is proposed as the PDF of P_{Rx} [10,14].

During the analysis described in Subsection II.E it has been observed that the K distribution is not suitable to describe the received optical signal better than the LN, G, or GG distribution. Therefore the K distribution is not considered any further within this publication. Very often scientists limit their research to scenarios where P_{Rx} is LN distributed because this simplifies the calculations and they accept the inaccuracies resulting from this [15]. In the following, the LN, G, and GG distribution functions are compared against sets of measured data to find the distribution that best fits these measurements and to evaluate whether the LN distribution can be used as a general distribution function. For this the definitions of the three distributions are given in the next section. For the visualization of distribution it is most common to use the PDF, but for statistical calculations and analysis the cumulative distribution function (CDF) is better suited than the PDF. The reason for this is that for deriving an emprical PDF from a measurement the histogram of this measurement has to be normalized so that its integral equals 1. The calculation of the integral can only be done by estimating it from a bar representation of the histogram, which is not very accurate in most cases. The empirical CDF (ECDF) does not have this source of inaccuracy because all data points of the curve have to be normalized by the maximum value for a correct representation; this can easily be done. Therefore both representations are given in the next section.

A generally used measure for describing the received power is the power scintillation index σ_P^2, which is the normalized variance of the received optical power P_{Rx}:

$$\sigma_P^2 = \frac{\langle P_{Rx}{}^2 \rangle}{\langle P_{Rx} \rangle^2} - 1, \tag{1}$$

where the brackets $\langle\ \rangle$ denote the ensemble average (sample mean). Without loss of generality it is assumed for the rest of this publication that P_{Rx} is given in a normalized form, i.e., $\langle P_{Rx} \rangle = 1$. Using this assumption σ_P^2 is equivalent to the sample variance of a normalized received power measurement and it is possible to relate most distributions directly to σ_P^2.

A. Log-Normal Distribution (LN)

The log-normal distribution is given by

$$\text{PDF: } f_{LN}(P_{Rx};\mu,\sigma^2) = \frac{1}{P_{Rx}\sqrt{2\pi\sigma^2}} e^{[\ln(P_{Rx})-\mu]^2/2\sigma^2}, \tag{2a}$$

$$\text{CDF: } F_{LN}(P_{Rx};\mu,\sigma^2) = \frac{1}{2} + \frac{1}{2}\,\text{erf}\left[\frac{\ln(P_{Rx})-\mu}{\sqrt{2\sigma^2}}\right], \tag{2b}$$

where μ is the mean and σ^2 is the variance of the natural logarithm of the received power, erf(x) is the error function, and σ^2 and μ are related to σ_P^2 by

$$\sigma^2 = \ln(\sigma_P^2 + 1), \tag{3a}$$

$$\mu = \ln(\langle P_{Rx}\rangle) - \frac{\sigma^2}{2} \overset{\langle P_{Rx}\rangle = 1}{\Rightarrow} -\frac{\sigma^2}{2}. \tag{3b}$$

B. Gamma Distribution (G)

The gamma distribution is given by

$$\text{PDF: } f_G(P_{Rx};k,\theta) = P_{Rx}{}^{k-1} e^{-P_{Rx}/\theta} \frac{1}{\theta^k \Gamma(k)}, \tag{4a}$$

$$\text{CDF: } F_G(P_{Rx};k,\theta) = \frac{\gamma\left(k, \dfrac{P_{Rx}}{\theta}\right)}{\Gamma(k)}, \tag{4b}$$

where $\gamma(a,x)$ denotes the lower incomplete gamma function, $\Gamma(z)$ denotes the gamma function, and the parameters $k>0$ and $\theta>0$ are related to measured values by

$$\theta = \sigma_P^2, \tag{5a}$$

$$k = \frac{1}{\sigma_P^2}. \tag{5b}$$

C. Gamma-Gamma Distribution (GG)

The gamma-gamma distribution is given by

$$\text{PDF: } f_{GG}(P_{Rx};\alpha,\beta) = \frac{2(\alpha\beta)^{\alpha+\beta/2}}{\Gamma(\alpha)\Gamma(\beta)} P_{Rx}^{\alpha+\beta/2-1} K_{\alpha-\beta}(2\sqrt{\alpha\beta P_{Rx}}), \tag{6}$$

where $K_n(x)$ is the modified Bessel function of the second kind and order n. The GG distribution also has a CDF in closed form [16], which is not given here because the closed form has a rather long and complex formulation that leads to numerical inaccuracies if implemented on a computer. In most cases it is more accurate to obtain the CDF by numerical integration of the PDF. The GG distribution has been developed by modeling the contributions of the atmospheric large-scale and small-scale scattering to optical scintillation as two independent G distributed processes [13]. Therefore the parameters α and β are directly related to the physical effects of large-scale and small-scale scattering, but nevertheless they cannot be directly related to measured P_{Rx} statistics. For estimating values for α and β the following relation can be used [5]:

$$\sigma_P^2 = \frac{1}{\alpha} + \frac{1}{\beta} + \frac{1}{\alpha\beta}. \tag{7}$$

Additionally it can be seen from Eqs. (6) and (7) that α and β have symmetrical effects on the distribution. Therefore a certain ratio r must exist that relates α to β:

$$\beta = r\alpha, \quad 0 \leqslant r \leqslant 1,$$

$$\sigma_P^2 = \frac{1}{\alpha} + \frac{1}{r\alpha} + \frac{1}{r\alpha^2}. \tag{8}$$

D. Experimental Data

For the analysis of the distribution of P_{Rx}, several measurements from mobile free-space optical communication demonstrations have been used. The selected measurements represent some typical areas where FSO links are currently deployed. These are a relatively short horizontal link over ground, a horizontal link of several kilometers over sea, and a downlink from a low-Earth-orbiting satellite that has a slant path through the atmosphere.

Measurement ATENAA: The short horizontal near-ground link was demonstrated in January 2007 in the ATENAA project funded by the European Union [17]. The aim of the ATENAA project was to demonstrate the applicability of optical wireless communications for airborne links. For this demonstration an optical simplex link was established between the optical ground station of the German Aerospace Center (DLR) in Oberpfaffenhofen, Germany, and a plane-emulating vehicle on the taxiway of the nearby airport. The wavelength was 808 nm with a beam power of 500 mW and a link distance ranging from 1200 to 1400 m. The weather conditions on the test day were overcast, partly sunny, wind 2 knots SW, relative humidity 81%, temperature 5°C, area partly covered by snow, some light rain showers. The beam full width half-maximum (FWHM) divergence angle was set to 15 mrad. The receiving aperture had a diameter of 8.5 cm and the modulation format was

non-return-to-zero on–off keying (NRZ-OOK). The link was used to transmit a User Datagram Protocol (UDP) video stream to the plane emulator with a data rate of 125 Mbits/s. The stream was secured by frame layer forward error correction.

Measurement LCT-Marine: The Laser Communication Terminal for Marine Environment (LCT-Marine) was demonstrated in June 2008 by Carl Zeiss Optronics on the Baltic Sea. The bidirectional link was established between a fixed ground station close to the coastline and a vessel. The link distance varied in this scenario from 3 to over 20 km. The weather conditions on the test day were partly cloudy, moderate visibility, water temperature 16°C, air temperature 17°C to 20°C, wind speed light air to gentle breeze. The communication wavelength was 1550 nm with a mean beam power of 200 mW and a FWHM divergence angle of 2.3 mrad. An NRZ-OOK modulated signal was used to transfer fast Ethernet data frames at a rate of 125 Mbits/s between the two stations (video conferencing and file transfer). The maximum height above ground/sea was 13 m at the ground station. Later during the demonstration it was reduced to approximately 4 m when the fixed station was moved closer to the sea. The receiving aperture diameter of the powermeter used was 5 cm.

Measurement KIODO 40 cm: The satellite downlink was demonstrated for the Kirari's Optical Downlink to Oberpfaffenhofen (KIODO) trials, which were a joint project between the Japan Aerospace Exploration Agency (JAXA) and DLR [18]. During these trials nine successful optical downlinks were demonstrated in 2007 and 2009 from the Japanese Optical Inter-orbit Communications Engineering Test Satellite (OICETS) to the optical ground station of DLR in Oberpfaffenhofen, Germany. OICETS is a low-Earth-orbiting satellite with a Sun-synchronous orbit and an altitude of 610 km. The communication wavelength was 848 nm with a mean transmission power of 100 mW and a FWHM divergence angle of 5.5 μrad. The data rate was 50 Mbits/s with NRZ-OOK modulation. The link distance varied between 778 and 2542 km, and the receiving aperture for the measurements was 40 cm with a central obscuration of 13 cm. The weather conditions on the test nights were clear sky, good visibility, air temperature 8°C to 18°C, calm air to gentle breeze.

Measurement KIODO 5 cm: During the KIODO campaign some measurements were also done using a 5 cm receiving aperture. The rest of the scenario parameters were kept the same as for the KIODO 40 cm measurements.

The available data from all measurements has a total duration of over 50 min. During each measurement the transmission beam was interrupted for a short period of time to allow the measurement of the background light. For the terrestrial links this was achieved by blocking the beam in front of the transmitter, and for the KIODO downlinks, the satellite pointed the transmission beam away from the ground station. For the following analysis, first the recorded signal was searched for the short outages and the background light value was determined. In mobile scenarios the level of the background light can change rapidly due to the fast changing background scenery. Therefore only measurements have been used where multiple outages could be detected and where the background light values did only vary slightly over the whole measurement. The measured background light was then subtracted from the signal before it was normalized by its mean for further analysis. All measurements have been gathered within mobile scenarios where link parameters can change rapidly. To reduce the impact of this parameter change, all measurements were split into data blocks of 10 s duration. For the KIODO links there was still some link parameter variation contained in the data blocks, caused by the fast changing link distance. To remove this variation from the data, the mean value calculation for the measurement normalization in KIODO was done using a sliding average of 1 s.

Because the receiving aperture is collecting signal energy across its surface, it averages signal fluctuations if the spatial scale of these intensity patterns (speckles) is smaller than the receiving aperture. With an increase of the receiving aperture, the experienced power fluctuations will decrease. This effect is known as aperture averaging [5]. A measure for the aperture averaging effect is the aperture averaging factor A_{AF}, which relates the normalized variance of the intensity σ_I^2 to the variance of the received power σ_P^2:

$$A_{AF} = \frac{\sigma_P^2}{\sigma_I^2}. \tag{9}$$

A_{AF} can take values between 0 and 1, where smaller values indicate more aperture averaging. Using the estimators for the aperture averaging factor given in [19,20] the estimate $\overline{A_{AF}}$ of the aperture averaging factor was derived for each power measurement. The derived values show that in ATENAA ($\overline{A_{AF}} \approx 0.06$) and KIODO 40 cm ($\overline{A_{AF}} \approx 0.05-0.25$) a fair amount of aperture averaging was taking place. In the LCT-Marine scenario only little aperture averaging ($\overline{A_{AF}} \approx 0.64-0.88$) was present. From this evaluation it can be seen that it is legitimate to assume that for existing FSO communication systems some aperture averaging will always be present and therefore P_{Rx} should be LN distributed. This is also valid for LCT-Marine because the aperture used for the measurements was limited to 5 cm, whereas the aperture of the communication system had a diameter of 12.5 cm and there-

fore the communication system was subject to more aperture averaging than measured. For KIODO 5 cm ($\overline{A_{AF}} \approx 0.99$) this assumption does not hold, but the 5 cm aperture was only installed for scientific use; for communications the 40 cm receiving aperture had to be used.

E. Fitting the Proposed Distributions to Experimental Data

For evaluating the assumption of the LN distributed P_{Rx}, the proposed distributions are fitted against the ECDF of the measured data. As mentioned above for LN and G the parameters are directly related to σ_P^2, but for the GG distribution a search for the ratio between the parameters α and β has to be done by using Eq. (8). Due to runtime issues, the search has to be stopped after a limited number of search iterations and therefore will not return the best-fitting parameters for the GG distribution, but the fit should be good enough to determine whether GG gives a better fit than LN or G. A positive side effect of this limitation is that it will be very unlikely that the found GG distribution will give the same fit as the G distribution (which should be possible in theory) and therefore it is possible to reveal cases where G is sufficient to describe the PDF of the received power.

For the evaluation of the fitting quality statistical tests like the Kolmogorov–Smirnov test are commonly used [21]. Such tests require that the measurement and the fitted distribution function are statistically independent. This requirement is not valid in the presented case because the distribution parameters are calculated from the values of the measurement. Therefore other techniques have to be used for evaluating the fitting quality. The fitting error between measurement and distribution function can be calculated by

$$e = F_M(P_{Rx}) - F(P_{Rx}), \tag{10}$$

where $F_M(P_{Rx})$ denotes the ECDF of the measurement and $F(P_{Rx})$ the CDF of the fitted distribution. For evaluating the quality of the fit, the following error measures can be used besides others [22]:

$$e_{rms} = \sqrt{\langle e^2 \rangle}, \tag{11}$$

$$e_{abs} = \max(|e|), \tag{12}$$

$$e_{rel} = \left\langle \frac{e}{F(P_{Rx})} \right\rangle. \tag{13}$$

The root mean square of the error (e_{rms}) is a measure that evaluates the quality of the fit over the whole range and is not sensible to single points where the two curves do not match. For detecting single points where the two curves do not match, the maximum absolute error (e_{abs}) can be used. e_{rms} and e_{abs} are linear measures, which give more weight to regions where larger values are present and fitting errors to the lower tail of the ECDF ($P_{Rx} < 1$) will be more or less ignored. The lower region of the ECDF is the region that is responsible for most communication errors, so it is desirable to ensure a good fit within this part of the ECDF. The relative error (e_{rel}) can be used for this.

For the evaluation of the fits, e_{rms} and e_{abs} have been used to verify that all three distributions give fits with approximately the same overall quality. This evaluation has shown that e_{rms} and e_{abs} are always in the same range for all three distributions with a mean value of 0.04 for e_{abs} and 0.02 for e_{rms} over all measurements (see Table I for more details). Since the overall fitting quality of the three distributions is nearly the same, e_{rel} has been used to identify the best-fitting distribution for all measurements. The mean values of e_{rel} for each measurement campaign are given in Table I. The final result of the evaluation process is given in Table II. To determine the turbulence regime given in the two tables, the estimators given in [19,20] have been used. During the analysis the following observation was made: For KIODO it can be observed that the turbulence strength depends on the elevation angle ϵ to the satellite. For $\epsilon < 10°$ moderate to strong turbulence is present, which changes to weak turbulence for larger ϵ. Regarding the best-fitting distribution, the evaluation has given the following results:

1) There is no single distribution that gives the best fit for all cases.
2) The best fitting distribution is independent of the turbulence strength.
3) The G distribution most often gives the best fit for $\epsilon > 10°$ in KIODO 40 cm, but rarely in the other, horizontal scenarios. For $\epsilon < 10°$ GG gives a better fit in KIODO 40 cm.
4) For ATENAA and LCT-Marine LN provides the best fit.
5) If the evaluation were done only between GG and LN, the evaluation result would not change.
6) Table I shows that all three distributions give fits with nearly the same overall fitting quality (e_{abs}, e_{rms}).

By visual inspection of the curve fits (e.g., Fig. 1), the following additional observations were made:

7) For KIODO the G distribution gives a good fit over the whole CDF, whereas LN tends to slightly underestimate the tails and overestimates the center of the CDF, especially for low elevation angles. Nevertheless, the difference between the distributions is very small, so all three distributions can be considered as accurate enough for simulations of optical downlinks.
8) The difference between the LN and GG fits is

TABLE I
EVALUATION OF THE OVERALL FITTING QUALITY OF THE THREE DISTRIBUTIONS[a]

Measurement Campaign	Estimated Turbulence Regime	σ_p^2	Error Measure	LN	G	GG
ATENAA	Weak	—	$\langle e_{rms} \rangle$	—	—	—
			$\langle e_{abs} \rangle$	—	—	—
			$\langle e_{rel} \rangle$	—	—	—
ATENAA	Moderate–strong	0.07–0.21	$\langle e_{rms} \rangle$	**0.01**	**0.01**	**0.01**
			$\langle e_{abs} \rangle$	**0.02**	0.03	**0.02**
			$\langle e_{rel} \rangle$	**0.13**	0.58	0.29
KIODO 40 cm	Weak ($\epsilon > 10°$)	0.00–0.13	$\langle e_{rms} \rangle$	**0.02**	**0.02**	0.03
			$\langle e_{abs} \rangle$	0.04	**0.03**	0.05
			$\langle e_{rel} \rangle$	0.08	**0.05**	0.18
KIODO 40 cm	Moderate–strong ($\epsilon < 10°$)	0.13–0.48	$\langle e_{rms} \rangle$	0.02	**0.01**	**0.01**
			$\langle e_{abs} \rangle$	0.04	0.02	**0.01**
			$\langle e_{rel} \rangle$	0.11	0.04	**0.03**
KIODO 5 cm	Weak ($\epsilon > 10°$)	0.05–0.69	$\langle e_{rms} \rangle$	**0.01**	**0.01**	**0.01**
			$\langle e_{abs} \rangle$	0.03	0.02	**0.01**
			$\langle e_{rel} \rangle$	0.07	0.06	**0.03**
KIODO 5 cm	Moderate–strong ($\epsilon < 10°$)	0.93–1.33	$\langle e_{rms} \rangle$	**0.02**	0.05	0.03
			$\langle e_{abs} \rangle$	**0.04**	0.11	0.06
			$\langle e_{rel} \rangle$	**0.09**	0.37	0.15
LCT-Marine	Weak	0.04–0.83	$\langle e_{rms} \rangle$	**0.01**	**0.01**	**0.01**
			$\langle e_{abs} \rangle$	**0.02**	0.04	0.03
			$\langle e_{rel} \rangle$	**0.07**	0.33	0.16
LCT-Marine	Moderate–strong	0.84–2.65	$\langle e_{rms} \rangle$	**0.02**	0.05	0.03
			$\langle e_{abs} \rangle$	**0.06**	0.13	0.07
			$\langle e_{rel} \rangle$	**0.09**	0.98	0.40

[a]The table gives the mean values of the error metrics for all fits within the given scenarios.

marginal in all cases, so both distributions should give a good model for all three scenarios.

This evaluation shows that it is sufficient to use either LN or GG for modeling the FSO communication channel. Based on the observations made, the fact that it is the best-fitting distribution according to theory (if aperture averaging is present) and because its parameters are directly related to σ_P^2, the LN distribution was selected as the PDF of the channel model. For KIODO this decision is justified by the small differences between GG and LN.

III. SPECTRAL CHARACTERISTICS OF THE RECEIVED OPTICAL POWER

Based on the work of Tatarskii [23] and Ishimaru [24], Andrews and Phillips [5] used Taylor's frozen turbulence hypothesis for describing the temporal

TABLE II
BEST-FIT RESULTS GROUPED BY MEASUREMENT CAMPAIGN AND ESTIMATED TURBULENCE REGIME[a]

Measurement Campaign	Estimated Turbulence Regime	σ_p^2	LN	G	GG	#samples
ATENAA	Weak	—	—	—	—	0
ATENAA	Moderate–strong	0.07–0.21	**55%**	25%	20%	20
KIODO 40 cm	Weak ($\epsilon > 10°$)	0.00–0.13	0%	**95%**	5%	106
KIODO 40 cm	Moderate–strong ($\epsilon < 10°$)	0.13–0.48	0%	36%	**64%**	22
KIODO 5 cm	Weak ($\epsilon > 10°$)	0.05–0.69	13%	7%	**80%**	46
KIODO 5 cm	Moderate–strong ($\epsilon < 10°$)	0.93–1.33	**56%**	0%	44%	9
LCT-Marine	Weak	0.04–0.83	**57%**	8%	35%	37
LCT-Marine	Moderate–strong	0.84–2.65	**73%**	0%	27%	40

[a]The columns LN, G, and GG show how often each distribution produced the best fit. The column #samples shows how many measurement samples have been available in each scenario.

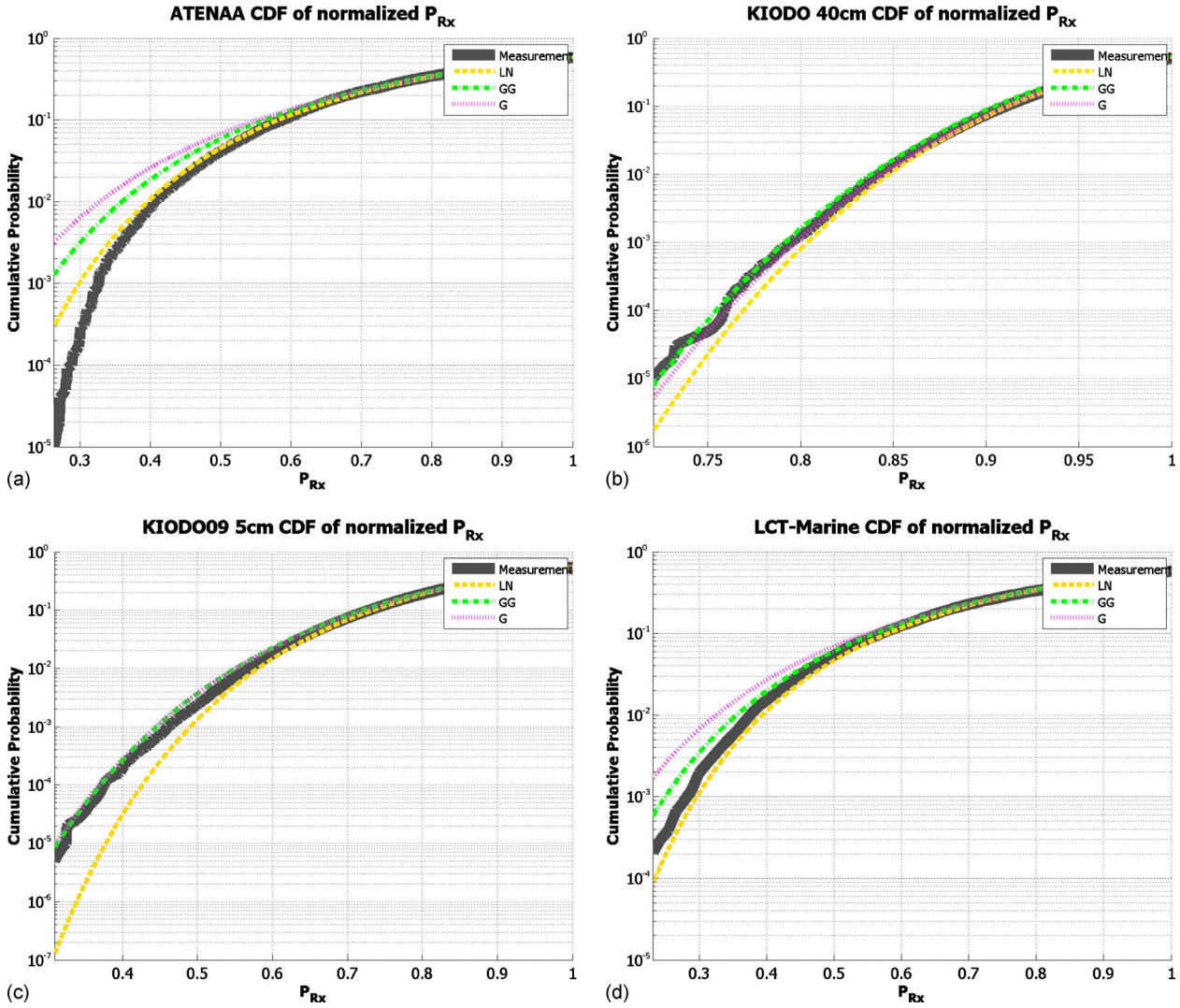

Fig. 1. (Color online) Exemplary plots for the fitting quality of the three distributions. Top left, ATENAA; top right, KIODO 40 cm; bottom left, KIODO 5 cm; bottom right, LCT-Marine. The lower tail ($P_{Rx} <= 1$) of the CDF is plotted on a semilogarithmic scale for making the small fitting errors in this region visible. This region is of major interest for simulating the fading behavior of the received power.

spectrum of the optical signal for point receivers. According to this theory a characteristic frequency f_t exists that divides the spectrum of the received power into two parts. The part below f_t has a flat PSD and for the part above f_t the PSD decays by $f^{-8/3}$, which results in −27 dB/s for higher frequencies. f_t can be approximated by

$$f_t = \frac{V_\perp}{\sqrt{L/k}}, \tag{14}$$

where $V_\perp$ is the mean transverse wind speed, L is the propagation distance, and k is the wave number ($=2\pi/\lambda$). For nonpoint receivers, which are typically the case for communication systems, the received power should be shifted toward lower frequencies and a deviation from the theoretical spectrum should be visible [5] as shown in Fig. 2. The theoretical PSD gives an estimate of the shape of the measured PSD,

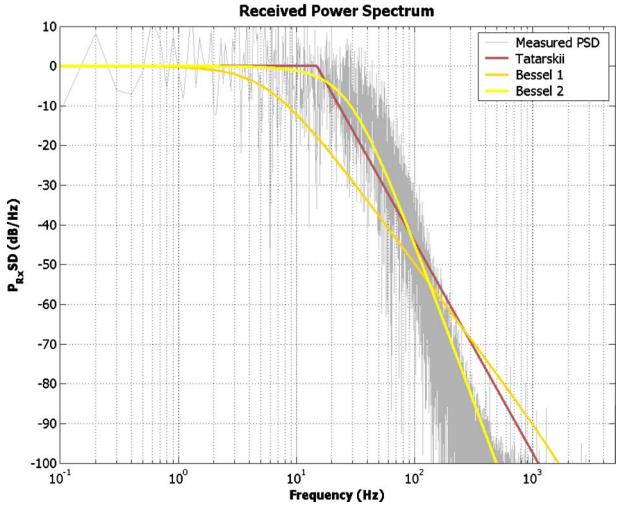

Fig. 2. (Color online) Exemplary comparison of a measured PSD, the PSD according to theory (Tatarskii), and first-order (Bessel 1) and second-order Bessel filters (Bessel 2). This plot is taken from a LCT-Marine measurement.

but it cannot be used for modeling it in more detail. The measured PSD has a long transition with a slope flatter than the theoretical PSD. After a certain point the slope gets steeper than predicted by theory. This shape is supposed to be caused by aperture averaging, which has an additional low-pass filtering effect on the signal, as mentioned before. To describe the filtering process of the atmosphere in a practical way, different generally available digital filters (Bessel, Butterworth, Chebyshev Type 1 and 2, and elliptic) are evaluated for reproducing the measured PSD from a series of white Gaussian noise. The algorithm used for generating the PSD is described in Section IV. The use of filters that are available in most signal processing libraries has the advantage that there are also filter design tools available that allow for on-the-fly design of these filters. This is, for example, needed for a channel simulator implementation where channel conditions can change during the runtime. During this evaluation the Bessel filters have been shown to give the best results. Additionally it has been observed that the filter parameters do not correlate with σ_P^2 and there is no correlation between properties from the communication scenario and the filter type or order. However, the derived cutoff frequencies seem to support Eq. (14). For the KIODO 40 cm and KIODO 5 cm measurements f_t is large compared with the two other scenarios because of the high relative velocity between the satellite and the ground station. For ATENAA and LCT-Marine the cutoff frequencies stretch approximately over the same frequency range, which seems plausible as both scenarios should have experienced similar wind speeds.

The evaluation results are given in Table III. The table is ordered first by the communication scenario and then by the occurrence percentage of the filter type given in the last column. The evaluation shows that for scenarios with a fair amount of aperture averaging (ATENAA, KIODO 40 cm) a first-order Bessel filter gives the best fit, whereas in scenarios with less aperture averaging (LCT-Marine, KIODO 5 cm) a second-order Bessel filter gives better results.

TABLE III
SETS OF DIGITAL FILTERS FITTING THE ANALYZED MEASUREMENTS

Scenario (#samples)	Filter	Order	f_C (Hz)	%
ATENAA (20)	Bessel	1	20–242	100
	Tatarskii	—	—	0
	Bessel	2	—	0
KIODO 40 cm (128)	Bessel	1	252–5702	61
	Tatarskii	–	80–1012	26
	Bessel	2	880–10000	13
KIODO 5 cm (55)	Tatarskii	–	159–535	60
	Bessel	2	1770–5807	24
	Bessel	1	577–2461	16
LCT-Marine (21)	Bessel	2	86–341	61
	Tatarskii	–	0–24	39
	Bessel	1	–	0

IV. GENERATING RECEIVED POWER VECTORS FOR NUMERICAL SIMULATIONS

Based on the work presented in the previous sections it is possible to generate time series of P_{Rx} without fully specifying the physical characteristics of the scenario. If the basic parameters of the communication scenario are known, e.g., location, link distance, time, it is possible to use established methods or databases for link budget calculation and to derive expected values for σ_P^2 and $\langle P_{Rx}\rangle$ [5]. With these two parameters the PDF of the expected received signal is specified and the method described in [25] can be used to generate a random signal with the specified properties.

A. Signal Generation Algorithm

The PDF of the received signal can be approximated by a LN distribution. In statistics the LN distribution can be described as a set of variables of which the logarithm is normally distributed. The normal distribution is given by

$$\text{PDF: } f_N(x;\mu,\sigma^2) = \frac{1}{\sqrt{2\pi\sigma^2}} e^{(x-\mu)^2/2\sigma^2}, \tag{15a}$$

$$\text{CDF: } F_N(x;\mu,\sigma^2) = \frac{1}{2} + \frac{1}{2}\,\text{erf}\left(\frac{x-\mu}{\sqrt{2\sigma^2}}\right), \tag{15b}$$

where μ is the mean value and σ the standard deviation of the distribution. If $X_{1,\ldots,n}$ is a set of normally distributed variables with size n and parameters μ and σ, then $Y_{1,\ldots,n}=e^{X_{1,\ldots,n}}$ will give a log-normally distributed set of variables with parameters μ and σ. Based on this, a series of P_{Rx} can be created in the following way. First a set of normally distributed variables $X_{1,\ldots,n}$ with certain μ and σ is generated. If this set is interpreted as a time series with a specified sample frequency, its PSD corresponds to the PSD of white Gaussian noise, which is flat over the whole frequency spectrum. By applying a filter to the set, its PSD can be changed to a desired shape. It is important to note that this filtering does not change the normal distribution type of the generated set, but it changes μ and σ of its distribution. To restore the original values of the parameters or to change them to other values, linear functions can be applied without changing the PSD or the normal distribution characteristics. The set with a specified normal distribution and a specified PSD can then be transformed to a LN

distributed set by applying the exponential function $\exp(X_{1,\ldots,n})$ to it. This step changes slightly the PSD of the generated time series, so the transfer function of the applied filter will be different from the PSD of the generated time series. Knowledge about σ_P^2 and $\langle P_{Rx}\rangle$ can be gained from the link budget calculations and therefore the described steps can be used in combination with Eq. (3) to generate LN distributed samples of P_{Rx} with a specified PDF and PSD. A suitable filter can be derived from Table III. The algorithm is illustrated in Fig. 3 and described as follows:

1) Calculate μ and σ^2 from $\langle P_{Rx}\rangle$ and using Eq. (3).
2) Generate a set of normally distributed variables $X_{1,\ldots,n}$ with μ and σ^2.
3) Select a filter from Table III according to the communication scenario and apply it to $X_{1,\ldots,n}$.
4) Apply linear operations to $X_{1,\ldots,n}$ to restore the calculated values for μ and σ^2.
5) Apply the exponential function to $X_{1,\ldots,n}$.

For most simulations it will be sufficient to select a first-order Bessel filter and vary its cutoff frequency from 1 to 400 Hz for links with slowly moving partners and from 200 to 6000 for links with higher dynamics.

B. Accuracy of the Algorithm

For design of FMT it is important to have good knowledge of the expected fade durations and their distribution. The ITU gives a recommendation about important fade duration statistics and their use for FMT design in [26]. In the following section, the term fade duration (d_F) is defined as the time interval between two crossings (down and up) of a threshold level P_T in the received signal. For FSO systems no generally used definition of this threshold level exists. For this publication it is assumed that the design goal of FSO communications systems is to achieve a certain $\langle P_{Rx}\rangle$ at the receiver. The value of $\langle P_{Rx}\rangle$ is set to a value fulfilling the system requirements, e.g., a long-term bit error probability for the received signal of 10^{-9}. With this understanding it is possible to define a fade as a drop in the received power below the targeted $\langle P_{Rx}\rangle$ and therefore $P_T=\langle P_{Rx}\rangle$.

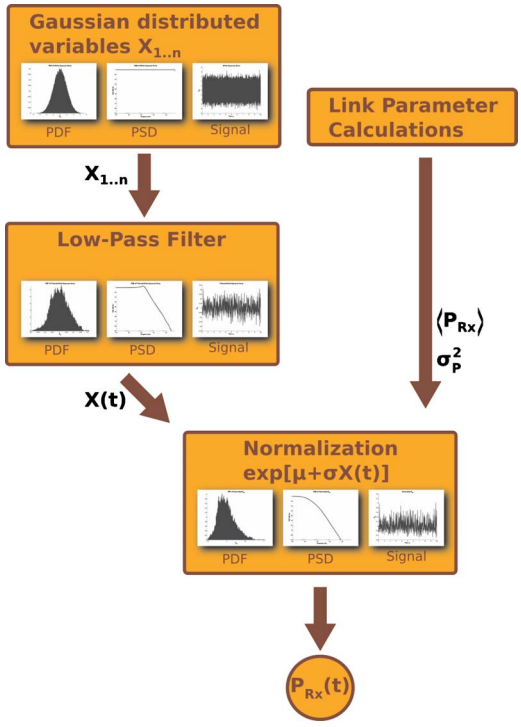

Fig. 3. (Color online) Schematic drawing of the proposed algorithm for generating time series of received power.

For describing the fade duration the ITU gives the following two measures based on the CDF of the fade duration:

1) Fade duration occurrence probability, that is, the probability of occurrence of fades of duration d_F longer than a given duration threshold D:

$$P(d_F > D) = \frac{N(d_F|d_F > D)}{N(d_F)}, \tag{16}$$

where $N(x)$ denotes the number of occurrences of x.

2) Cumulative fade duration exceedance probability, that is, the probability that, if a fade occurs, it has a duration $d_F > D$:

$$F(d_F > D) = \frac{\sum_i (d_{F,i}|d_{F,i} > D)}{\sum_i d_{F,i}}. \tag{17}$$

The two given measures can be used to describe the distribution of the fade durations, but they do not describe the occurrence of the fades. For describing the occurrence of fades, the received signal can be segmented into fades ($P_{Rx} < P_T$) and surges ($P_{Rx} \geq P_T$).

3) Probability of fade,

$$P(P_{Rx} < P_T) = \frac{\sum_i d_{F,i}}{D_{tot}}, \tag{18}$$

where D_{tot} is the total duration of the measurement.

These three measures are used to evaluate the agreement between the measurements and the generated P_{Rx} vectors. To illustrate the results of this evaluation, exemplary plots of the fade duration measures are given in Fig. 4. The evaluation results show that the proposed algorithm simulates the probability of fade with an e_{rms} of less than 0.03. For fade duration occurrence ($e_{rms} < 0.04$) and exceedance ($e_{rms} < 0.01$) the accuracy is also within an acceptable range. Despite all simplifications made, the algorithm can gen-

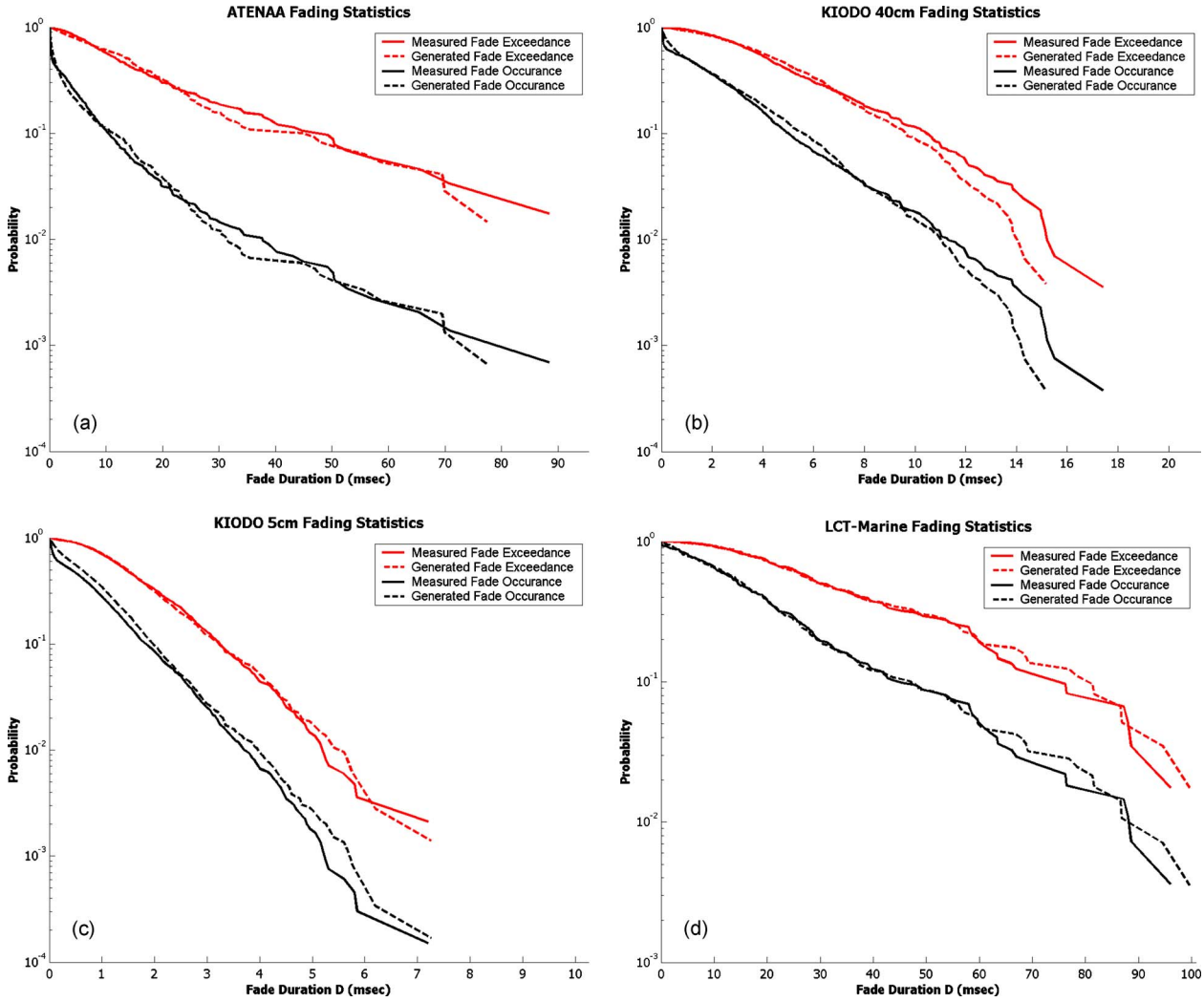

Fig. 4. (Color online) Fade duration occurrence and exceedance probability plots. These are exemplary plots from all four scenarios to illustrate the achieved accuracy. Top left, ATENAA; top right, KIODO 40 cm; bottom left, KIODO 5 cm; bottom right, LCT-Marine.

erate P_{Rx} series that are very similar to the measured values. The fade duration is mainly determined by $V_{\perp}$, which varies significantly over time, and therefore the simulation runs made for designing a FMT have to cover a wide range of fade duration distributions for evaluating the FMT's robustness against the changing link conditions. The cutoff frequency of the filter used for simulations should be varied over the ranges given in Table III.

C. Using Received Power Vectors for Simulation of FSO Communications

For completeness in the following section it is shown how the power vectors generated can be used for calculating the packet loss probability (PLP), which is often required for conducting simulations. First the bit error probability (BEP) has to be calculated from the power vector. For this a receiver model is needed. Such a model was developed for IM/DD receivers in [27]. In this model the IM/DD receiver is defined by its characteristic power P_0 and a form factor ξ. The BEP for a given P_{Rx} can then be calculated by

$$\mathrm{BEP}(P_{Rx}) = \frac{1}{2}\,\mathrm{erfc}\left[\frac{Q(P_{Rx})}{\sqrt{2}}\right] \tag{19}$$

with

$$Q(P_{Rx}) = \frac{P_{Rx}/P_0}{1+\sqrt{1+\xi P_{Rx}/P_0}}. \tag{20}$$

This model can be used during system design and link budget calculation for calculating the $\langle P_{Rx}\rangle$ that is required to achieve a desired long-term BEP by rewriting Eqs. (19) and (20) to

$$Q(\mathrm{BEP}) = \sqrt{2}\times \mathrm{erfc}^{-1}(2\mathrm{BEP}), \tag{21}$$

$$\langle P_{Rx}\rangle = [\xi Q(\mathrm{BEP})^2 + 2Q(\mathrm{BEP})]P_0. \tag{22}$$

At DLR three receivers have been parameterized for this model and can be used in simulations or calculations. These receivers are CAPANINA Rx (APD, 1550 nm, 1250 Mbits/s), which is a custom build by DLR; CDX RFE01b (APD, 1550 nm, 155 Mbits/s), a receiver available from Codex GmbH & Co. KG; and Fujitsu FRM5W621KT/LT (APD, 1550 nm, 622 Mbits/s), which is available from Fujitsu. The derived parameters are given in Table IV. For optical wireless communications it can be assumed that the received power is constant over the whole transmission of a data packet. This assumption is based on a simple calculation. The largest packets present in today's networks have sizes of about 1500 bytes. For a relatively low data rate of 125 Mbits/s this results in a packet duration of about 0.1 ms, which is less than the generally assumed fade duration of several milliseconds. Thus it is legitimate to calculate the PLP by

$$\mathrm{PLP}(P_{Rx}, n_P) = 1 - [1 - \mathrm{BEP}(P_{Rx})]^{n_P}, \qquad (23)$$

where n_P denotes the number of bits per packet. Another possibility to use the proposed model is to convert the generated power vectors into attenuation vectors to drive a variable attenuator. This attenuator can then be used as a channel simulator for the development and testing of hardware, e.g., an optical IM/DD receiver, without the need for a long-range FSO test link.

V. Conclusion

In this work a simple way to model the fading behavior of the free-space optical signal has been presented. The proposed methodology is easy to implement and does not require deep knowledge of the physical channel. The model is based on the estimation of the two input parameters σ_P^2 and $\langle P_{Rx} \rangle$ and the selection of a suitable low-pass filter from Table III. For most communication scenarios a first-order Bessel filter will produce good results. The PDF of the received signal is determined to be the log-normal distribution. This decision is based on reports in the literature as well as on analysis of measured data. It has been shown that the fading behavior of the received power is modeled with good agreement to measured data. For the development of FMT the achieved accuracy is sufficient. The presented approach can be used as a channel simulator inside a computer or similar device or it can be used to generate attenuation vectors to drive variable attenuators for conducting simulations in the optical or electrical domain. Finally a way that time series of received power can be used for simulations is given, so the presented work can directly be used for the implementation of a simulator.

TABLE IV
Derived Receiver Model Parameters for Selected Optical Receivers

Receiver	$P_0(nW)$	ξ
CAPANINA RX	4.19	0.46
CDX RFE01b	0.92	0.78
Fujitsu FRM5W621KT/LT	1.35	0.80

Acknowledgments

The author thanks the ATENAA Consortium, Carl Zeiss Optronics, Codex GmbH & Co. KG, and JAXA for good cooperation within the projects and for the opportunity to use the gathered data for the analysis done within this work. He also thanks his colleague Dr. Nicolas Perlot for all the inspiring discussions about scintillation theory.

References

[1] J. Horwath, M. Knapek, B. Epple, M. Brechtelsbauer, and B. Wilkerson, "Broadband backhaul communication for stratospheric platforms: the stratospheric optical payload experiment (STROPEX)," *Proc. SPIE*, vol. 6304, paper 63041N, 2006.

[2] N. Perlot, M. Knapek, D. Giggenbach, J. Horwath, M. Brechtelsbauer, Y. Takayama, and T. Jono, "Results of the optical downlink experiment KIODO from OICETS satellite to optical ground station Oberpfaffenhofen (OGS-OP)," *Proc. SPIE*, vol. 6457, paper 645704, Mar. 2007.

[3] D. W. Young, J. E. Sluz, J. C. Juarez, M. B. Airola, R. M. Sova, H. Hurt, M. Northcott, J. Phillips, A. McClaren, D. Driver, D. Abelson, and J. Foshee, "Demonstration of high data rate wavelength division multiplexed transmission over a 150 km free space optical link," in *IEEE Military Communications Conference, 2007. MILCOM 2007*, Oct. 2007, pp. 1–6.

[4] L. C. Andrews, R. L. Phillips, and C. Y. Hopen, *Laser Beam Scintillation With Applications*, SPIE Press Monograph Series. Bellingham, WA: SPIE Optical Engineering Press, 2001, vol. PM99.

[5] L. C. Andrews and R. L. Phillips, *Laser Beam Propagation Through Random Media*, 2nd ed., SPIE Press Monograph Series. Bellingham, WA: SPIE Optical Engineering Press, 2005, vol. PM152.

[6] H. Henniger, B. Epple, S. D. Milner, and C. C. Davis, "Coding techniques to mitigate fading on free-space optical communication links," *Proc. SPIE*, vol. 7091, paper 70910C, Aug. 2008.

[7] R. Purvinskis, D. Giggenbach, H. Henniger, N. Perlot, and F. David, "Multiple-wavelength free-space laser communications," *Proc. SPIE*, vol. 4975, pp. 12–19, 2003.

[8] A. Biswas and S. Lee, "Ground-to-ground optical communications demonstration," Jet Propulsion Laboratory, Pasadena, CA, Telecommunications and Mission Operations Progress Rep. 42-141, May 2000.

[9] X. Zhu and J. M. Kahn, "Free-space optical communication through atmospheric turbulence channels," *IEEE Trans. Commun.*, vol. 50, no. 8, pp. 1293–1300, Aug. 2002.

[10] F. Strömqvist Vetelino, C. Young, and L. C. Andrews, "Fade statistics and aperture averaging for Gaussian beam waves in moderate-to-strong turbulence," *Appl. Opt.*, vol. 46, no. 18, p. 3780, June 2007.

[11] G. Parry, "Measurement of atmospheric turbulence induced intensity fluctuations in a laser beam," *J. Mod. Opt.*, vol. 28, no. 5, pp. 715–728, May 1981.

[12] L. C. Andrews and R. L. Phillips, "Measured statistics of laser-light scattering in atmospheric turbulence," *J. Opt. Soc. Am.*, vol. 71, no. 12, pp. 1440–1445, 1981.

[13] M. A. Al-Habash, L. C. Andrews, and R. L. Phillips, "Mathematical model for the irradiance probability density function of a laser beam propagating through turbulent media," *Opt. Eng.*, vol. 40, no. 8, pp. 1554–1562, Aug. 2001.

[14] N. Perlot and D. Fritzsche, "Aperture-averaging—theory and measurements," *Proc. SPIE*, vol. 5338, pp. 233–242, June 2004.

[15] A. K. Majumdar and J. C. Ricklin, Eds., *Free-Space Laser Communications: Principles and Advances*, Optical and Fiber Communications Reports. New York: Springer, Dec. 2008, vol. 2.

[16] L. C. Andrews and R. L. Phillips, *Mathematical Techniques for Engineers and Scientists*, SPIE Press Monograph Series. Bellingham, WA: SPIE Press, 2003, vol. PM118.

[17] C. Fuchs, H. Henniger, B. Epple, D. Giggenbach, M. Amirfeiz, M. Jentile, G. Di Nepi, F. Mazzi, and G. Martini, "Broadband communications for aeronautical networks: the ATENAA outer optical link validation," in *Proc. of 1st CEAS European Air and Space Conf.*, Sept. 2007.

[18] T. Jono, Y. Takayama, and N. Perlot, *Report on DLR-JAXA Joint Experiment—The Kirari Optical Downlink to Oberpfaffenhofen (KIODO)*. Japan Aerospace Exploration Agency, April 2007.

[19] L. C. Andrews, "Aperture-averaging factor for optical scintillations of plane and spherical waves in the atmosphere," *J. Opt. Soc. Am. A*, vol. 9, no. 4, pp. 597–600, 1992.

[20] J. H. Churnside, "Aperture averaging of optical scintillations in the turbulent atmosphere," *Appl. Opt.*, vol. 30, no. 15, pp. 1982–1994, May 1991.

[21] A. Papoulis and S. U. Pillai, *Probability, Random Variables, and Stochastic Processes*, 4th ed. McGraw-Hill, 2002.

[22] S. Jachner, K. G. v. d. Boogaart, and T. Petzoldt, "Statistical methods for the qualitative assessment of dynamic models with time delay (R package qualV)," *J. Stat. Software*, vol. 22, no. 8, pp. 1–30, 2007.

[23] V. I. Tatarskii, *Wave Propagation in a Turbulent Medium*. New York: McGraw-Hill, 1961.

[24] A. Ishimaru, *Wave Propagation and Scattering in Random Media*. New York: Academic, 1978.

[25] U. G. Gujar and R. J. Kavanagh, "Generation of random signals with specified probability density functions and power density spectra," *IEEE Trans. Autom. Control*, vol. 13, no. 6, pp. 716–719, Dec. 1968.

[26] "Prediction method of fade dynamics on Earth-space paths," International Telecommunication Union (ITU), Recommendation ITU-R P.1623-1, 2005.

[27] F. David, "Scintillation loss in free-space optic IM/DD systems," *Proc. SPIE*, vol. 5338, pp. 66–75, Jan. 2004.